Investigations on Pulse Broadening for Catalyst Screening in Gas/Liquid Systems

H. Pennemann, V. Hessel, H.-J. Kost, and H. Löwe
Institut für Mikrotechnik Mainz GmbH, 55129 Mainz, Germany

C. de Bellefon
Laboratoire Génie des Procédés Catalytiques, CNRS/ESCPE Lyon, F-69616 Villeurbanne, France

DOI 10.1002/aic.10150
Published online in Wiley InterScience (www.interscience.wiley.com).

In connection with the development of a complete screening setup for organometallic catalysis, a micromixer–tube setup was investigated to optimize its serial transient operation mode. Because homogeneously dissolved catalysts and substrates in the liquid phase of a gas/liquid system are pulse-injected into the two-phase system, our investigations aim in finding a minimum in the signal broadening and maximizing the number of experiments per unit of time. Within this context, investigations of the residence time distribution of the whole setup, as well as the individual contributions of its respective components toward signal broadening, were undertaken by determining the effects on the residence time distribution by the gas/liquid ratio, the orientation of the residence time loop and the total flow rate. © 2004 American Institute of Chemical Engineers *AIChE J,* 50: 1814–1823, 2004
Keywords: biphasic screening, gas/liquid dispersion, multiphase flow, foam, micromixer

Introduction

Miniaturized reactors have recently been the focus of increasing attention for screening purposes, in particular on finding new catalysts. Thus, most investigations so far have been related to the field of heterogeneous catalysis, in the finding of solid catalysts for gas-phase reactions. In this context, both highly parallel (Cong et al., 1999; Hoffmann et al., 1999, 2001; Rodemerck et al., 2000; Thomson et al., 2001; Zech et al., 1999, 2001) and, to a lesser extent, serial approaches (Besser and Prevot, 2000; Besser et al., 2001) have been used. The former are mostly taken for primary screening purposes, that is, analyzing the performance of a multitude of formerly unknown catalyst compositions. The latter are usually dedicated to secondary screening or process optimization in general, meaning the fast variation of process parameters while using one or a few given catalysts.

Correspondence concerning this article should be addressed to H. Pennemann at pennemann@imm-mainz.de.

Serial screening in microdevices has thus far scarcely been used for primary screening of heterogeneous catalysts and significantly less for investigating organic catalyzed reactions. For the latter, serial screening of multiphase processes in microdevices is of special interest because this allows the corresponding mass and heat transfer limitations to be overcome, thereby enabling a kinetically controlled operating regime. Indeed, first studies on the serial screening of both liquid/liquid and gas/liquid reactions, that is, the isomerization of allyl alcohol derivatives and the hydrogenation of Z-(α)-acetamidocinnamic methyl ester, were undertaken (de Bellefon et al., 2000).

The serial screening in the above-mentioned case was based on a gas/liquid dispersion flow generated continuously by the so-called slit interdigital micromixer (see Figure 2 below). To minimize the amount of reactant and catalyst, the combined solution of both was injected in terms of a pulse into the continuous liquid flow by use of an HPLC valve. Subsequently, this combined reactant and catalyst solution was dispersed by the micromixer. The generated two-phase flow acted like a carrier and conveyed the resulting reacting segment along the tubular reactor.

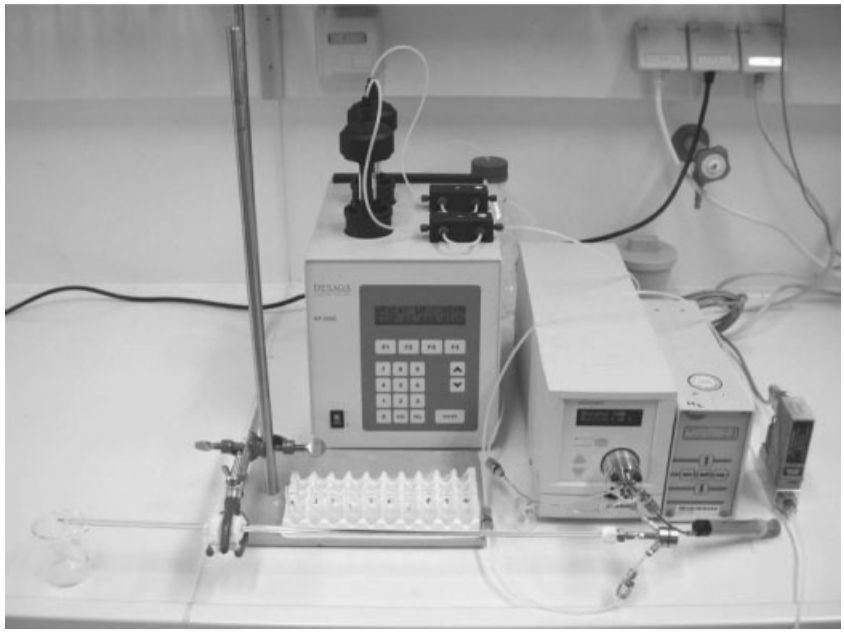

Figure 1. Micromixer–tube setup for transient catalyst screening.

The multiphase medium was a rigid foam, consisting of regular-shaped gas bubbles ("hexagon flow"; see Hessel et al., 1998), which was guided in a straight tube. More detailed investigations on such monodisperse foam structures and the governing process parameters for their generation were reported in Mathes and Plath (2001).

The previously cited reactions led to the formation of chiral products by homogeneously dissolved chiral transition-metal catalysts. Besides providing information on conversion, selectivity, and enantiomeric excess, these basic investigations also served as a source of characteristic data on the screening process itself. Among these, relevant parameters such as the test-throughput frequency, the ratio of useful to withdrawn experiments, the total sample consumption, and the amount of precious transition-metal catalyst consumed were described. In a recent work, it was found for a gas/liquid process that the maximum number of experiments that can currently be achieved amounts to about 40 per day. This translates to a duration of typically 12 min for each experiment assuming an 8-h operation (de Bellefon et al., 2002). Because it was known before starting the study reported in the present article that typical pulse time scales are also in the order of several minutes, the reduction of this parameter is crucial for further optimization of the serial-pulse screening technique described above.

There is no widespread fundamental knowledge on the time scale of pulses in microreactors, more particularly in "pulse history" (that is, the generation of pulses in microreactors and the signal broadening during a continuous-flow process). Although more application oriented, studies on three periodically operated reactions (with respect to reactant concentration) in a specially designed microstructured reactor revealed the time scale of pulses in gas media. Depending on the reaction investigated, it was shown that pulses with durations ranging from 30 s to several minutes were created. In connection with this, the effect of radial dispersion on flow profiles in microchannels was analyzed as a function of the diffusivity (Liauw et al., 2000; Walter and Liauw, 2000; Walter et al., 2001), with respect to the previous work of Taylor (1954) and Aris (1955).

Accordingly, it is the aim of the present article to provide information on the determination of the time scale of pulses with respect to the serial-pulse screening technique described above. Particularly, a mechanistic analysis of the origins of pulse broadening will be performed that allows one to draw conclusions on future reduction of pulse broadening and, thereby, to achieve faster serial catalyst screening.

Experimental

The setup used (Figure 1) consisted of a micromixer unit, which was connected to a residence time loop of variable length. The latter was a tube with an inner diameter of 2.2 mm and a length of either 50, 100, or 150 cm. The tube is made of glass so as to permit a visual inspection of the foam quality.

The main part of the setup was the micromixer with an LIGA-Inlay (Figure 2) (Ehrfeld et al., 1999), which was originally developed for an interdigital contacting of two miscible (Ehrfeld et al., 1999; Herweck et al., 2001) or immiscible liquids (Haverkamp et al., 1999; Herweck et al., 2001; Hessel et al., 1999). Recently, the capabilities in generating gas/liquid dispersions using this device were shown (Hessel et al., 1998; Mathes and Plath, 2001). The inlets of the mixer were connected to a nitrogen line with mass flow meters (EL-Flow, Bronkhorst HI-TECH, Ruurlo, The Netherlands) and an HPLC valve (Rheodyne 7000, Rheodyne, Rohnert Park, CA) with a piston pump (KP2000, Desaga Sarstedt-Gruppe, Wiesloch, Germany).

The HPLC valve was equipped with a 0.015-cm^3 sampling loop. As liquid phase, an aqueous solution of 0.01 mol/dm^3 sodium dodecyl sulfate (SDS) was used. The nitrogen/aqueous SDS solution system serves as a model system for the reaction system hydrogen/aqueous ethylene glycol and SDS used in de

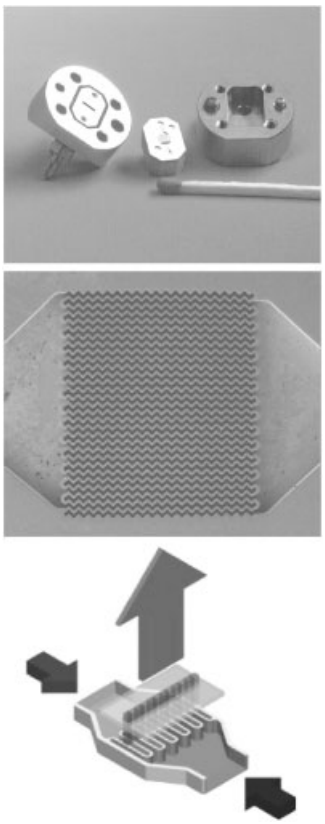

Figure 2. Disassembled micromixer with LIGA-inlay (left), SEM of the LIGA-inlay (middle), and mixing principle of the micromixer (right).

Bellefon et al. (2000). It was mainly chosen for giving ideal foams based on prior experience (Hessel et al., 1998; unpublished results). The tracer (0.01 g/cm^3 methyl blue in the above-mentioned aqueous SDS solution) was injected by use of a valve actuator (Valvemate™, Gilson, Middleton, WI). The described setup is the essential part of a totally automated screening setup, which is operated at the Laboratoire Génie des Procédés Catalytiques, CNRS-Lyon. In contrast to the automated setup, the samples in the present work were collected manually at successive intervals. Because of the high volume flows during some screening experiments a simple manual sampling was inadequate to collect the samples discretely, but rather resulted in a loss of a significant amount of sample volume. As a consequence, several rectangular cuvettes, typically 10–20, were placed tightly on a rack. This rack was moved with almost constant velocity with respect to the glass tube outlet. To determine the time intervals between the respective samplings, the ratio of sample weight to flow rate was calculated. After diluting the samples with 0.1% hydrochloric acid at a mass ratio 1:20, the concentration was detected at 604 nm using a UV/vis spectrometer (Hitachi U-3000, Hitachi, Singapore).

The Lambert–Beer law was shown to be valid for all methyl blue concentrations in the samples. It should be noted that the procedure yields residence times of the liquid phase, not the gas phase.

Because a HPLC sampling loop was used for the injection of the pulse into the screening setup, the starting pulse can be described as a rectangular input signal and the mean residence time as well as the variance can be calculated from the hydrodynamic data. The response to the rectangular input signal was determined at different measuring points of the setup (Figure 3). The first was positioned after the steel capillary, which connected the valve with the micromixer. It sums up the effect of the sample loop, the valve, and the steel capillary itself toward the pulse broadening. Further measuring points were after the micromixer and at different axial positions of the glass tube.

The pressure drop was measured with a pressure meter (P-40, Wagner, Offenbach/Main, Germany).

Results

Exit age distribution function E(t) in different segments of the system

From the achieved tracer concentrations of the collected samples the E function $E(t)$, the mean residence time $\bar{t}$, the variance σ_t^2, and the dimensionless variance σ_θ^2 are calculated using Eqs. 1–4.

Exit Age Distribution Function

$$E(t) = \frac{c_i(t)}{\sum_i c_i(t)\Delta t_i} \tag{1}$$

Mean Residence Time

$$\bar{t} = \sum_i t_i E_i(t)\Delta t_i \tag{2}$$

Variance

$$\sigma_t^2 = \sum_i (t_i - \bar{t})^2 E_i(t)\Delta t_i \tag{3}$$

Dimensionless Variance

$$\sigma_\theta^2 = \frac{\sigma_t^2}{\bar{t}^2} \tag{4}$$

Figure 3 shows the response of an injected pulse on its way through the setup. As expected, the height of the response signal declines, whereas the width increases over the course of time. The width increases from the hydrodynamically calculated 0.18 min of the sampling loop up to 0.6 min after the valve/capillary, to 0.9 min after the micromixer, and to 1.4 min after the 150-cm glass tube.

For a proper comparison of the pulse history and for a mechanistic analysis, one usually refers to the variance and the dimensionless variance. To apply these functions in the present case, one has to check whether they are consistent with the cumulative law. This is done by the calculation of the number of vessels by use of the tanks-in-series model. For the tubes, vessel numbers of 567 (50-cm tube), 1290 (100-cm tube), and 1808 (150-cm tube) are calculated. In contrast, for the valve/capillary the number of vessels amounts to 2, and for the mixer this value is only 1. Thus, only the tubes strictly conform to the cumulative law. This is also experimentally confirmed by the

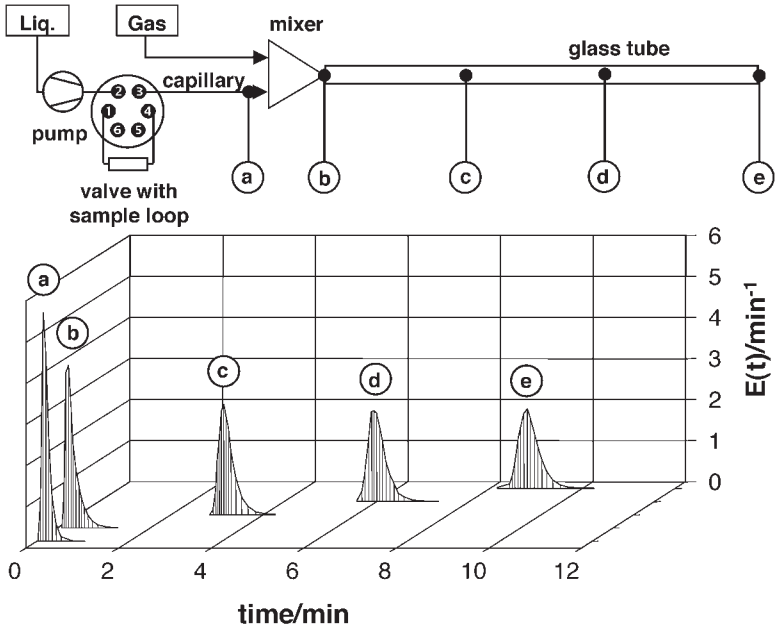

Figure 3. Exit age distribution function at different measuring points of the screening setup with 10 cm^3/h liquid flow rate and 0.5 cm^3/min gas flow rate.

linear increase of such derived variances with an extension of tube length. The low vessel numbers for the valve/capillary and mixer indicate a relatively substantial dispersion in both these parts of the setup, which implies that the above assumed cumulative behavior of mean residence times and variances is questionable. Accordingly, the exact individual contribution of these parts of the setup could be calculated only by a complex deconvolution of the corresponding exit age distribution functions.

The low vessel numbers of the valve/capillary and mixer, as well as the questioning of the cumulative behavior, may be related to their short residence time and are possibly attributable to other construction details, such as to complex fluid architecture. Because these are intrinsic properties, we propose to describe the subsequent changes of the functions σ_t^2 and σ_θ^2 when adding parts of the setup in a previously defined sequence and, for the sake of simplicity, to designate these changes by the component added. For instance, the individual contribution that occurs when adding a mixer is simply referred to as σ_t^2 ("mixer"), knowing that this variance does not precisely describe the σ_θ^2 correlation of the mixer itself but rather the connection of this component to another in a fixed order. This simplification is justified from the point of view that this study does not aim at analyzing virtual connections of valve/capillary, mixer, and tube. For instance, the analysis of a series of components starting with a tube, followed by mixer and valve/capillary, would make no sense because this does not correspond to any practical constructional or operational solution.

Following the simplified definition given above, one can calculate the individual contribution of the stepwise addition of every component toward the variances (Figure 4, top) and dimensionless variances (Figure 4, bottom).

In the top graph of Figure 4 it is shown that the variance is increased relatively little by the "valve/capillary" (factor 3.7

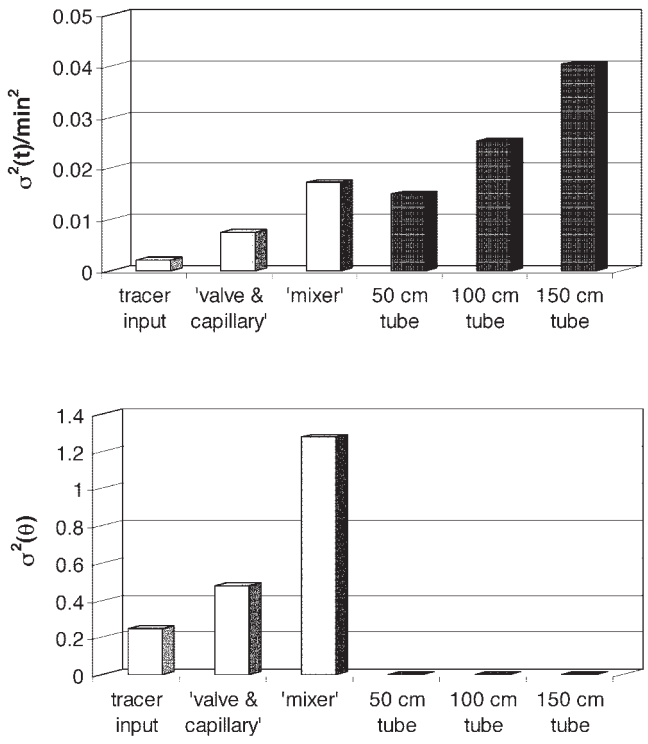

Figure 4. Individual contributions of the component parts to the variance (top) and the resulting dimensionless variances (bottom) of every component using a gas flow rate of 0.5 cm^3/min, a liquid flow rate of 10 cm^3/h, and different tube lengths.

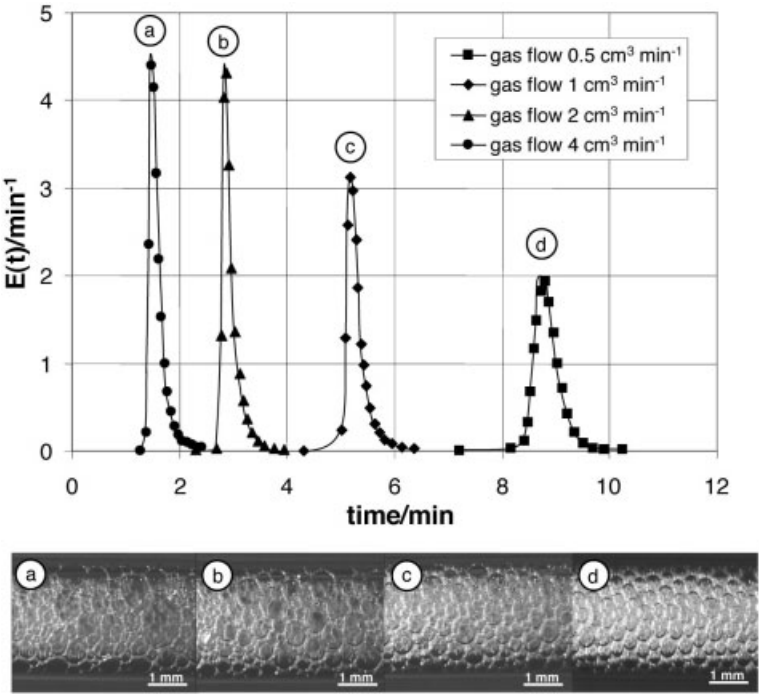

Figure 5. Correlation of the exit age distribution function and the liquid content of the foam using different gas/liquid ratios.

Liquid flow rate: 10 cm^3/h.

based on the hydrodynamically calculated variance of the sampling loop) but mainly by the "mixer" (factor 8.5) and the glass tube (factor 7.4, 12.5, and 19.9 depending on the tube length). This means that the variance of the primary tracer signal is increased approximately by the factor 33 when flowing through the whole setup.

For a true comparison of the equipment's parts concerning their contributions to the overall variance, it is necessary to take into account the mean residence time of each part (Eq. 4). The resulting dimensionless variances σ_θ^2 are illustrated in the bottom graph of Figure 4. It is evident that the principal part of the dimensionless variance stems from the addition of the "micromixer" and the "valve/capillary." In comparison with the "mixer" impact, the dimensionless variance of the glass tube is small.

Effect of the gas/liquid ratio on exit age distribution function and variance

Further investigations refer to the correlation between the gas/liquid ratio of the dispersion and the broadening of the pulse response. The motivation was to influence the rigidity of the foam by increasing the gas/liquid ratio. The latter leads to a drained foam, where the arbitrary mixing by convection of bubbles should be decreased by the foam framework.

The experiments were carried out with a constant liquid flow rate (10 cm^3/h) and different gas flow rates of 0.5, 1, 2, and 4 cm^3/min. Using these gas flow rates, the gas/liquid ratio increases from 75%, which is comparable to a density ratio of a face-centered cubic or a hexagonal lattice to gas/liquid ratios of 86, 92, and 96%. The higher gas flow rates result in a polyhedral appearance of the foam rather than a bubbly one (Figure 5).

It is clear that a higher gas flow rate involves a decrease of the mean residence time, although this decrease is found not to be linear (Figure 5). This may be explained by the fact that higher gas flow rates lead to higher pressure drops in the setup (see Table 2 below). The latter affects the total volume of the gas bubbles and thereby the residence time.

At a first glance, one can see in Figure 5 that high gas flow rates seem to be connected with a reduction of signal broadening of the respective pulses. However, for a proper comparison of these experimental results, the dimensionless exit age distribution function $E(\theta)$ has to be chosen. The latter is achieved by Eq. 5.

Dimensionless Exit Age Distribution Function

$$E(\theta) = \bar{t}E(t) \tag{5}$$

From Figure 6 it can be seen that the $E(\theta)$ function becomes wider and flatter when the gas flow is increased. This is accompanied by an increasing overall variance. To have a closer look at how the variance of the individual setup parts is influenced by the gas/liquid ratio of the foam, their individual contributions were calculated (Figure 7).

Figure 7 shows that for both mixer and glass tube the dimensionless variance increases with higher gas flow rates. With respect to the mean residence time, the mixer has the greatest effect on signal broadening.

These results indicate that a higher rigidity of the foam realized by a higher gas/liquid ratio is not helpful in minimizing the spread of the response signal. Furthermore, Figure 5 shows that the rigidity is also connected to a wider spread in bubble size, leading to a polyhedral shape of the foam. Ac-

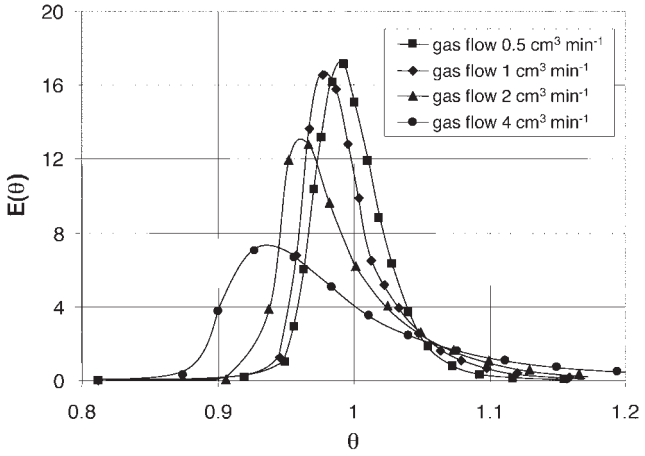

Figure 6. Dimensionless exit age distribution function using different gas/liquid ratios.

Liquid flow rate: 10 cm^3/h.

cordingly, one can also draw the conclusion that the micromixer is an absolutely essential part of the setup because such polyhedral foams can be made by simple mixing tees as well (but not bubbly foams, as illustrated by the image d in Figure 5).

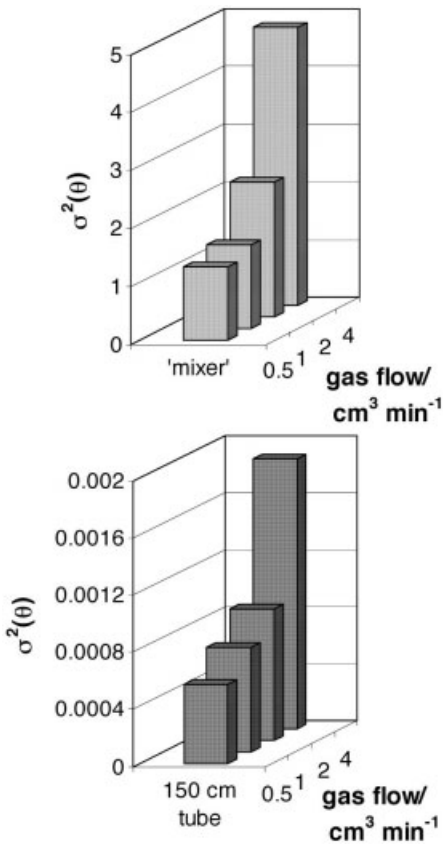

Figure 7. Dimensionless variance of the mixer and the tube with respect to different gas flow rates.

Liquid flow rate: 10 cm^3/h, tube: 150 cm.

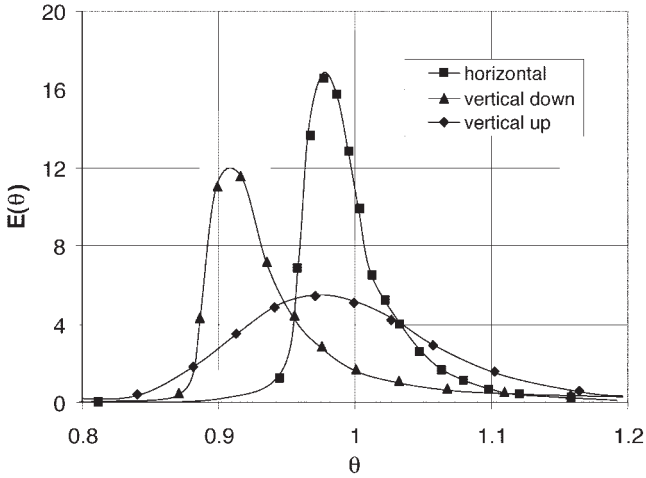

Figure 8. Dimensionless exit age distribution functions of setups with different stored glass tubes and flow directions.

Length: 150 cm, liquid flow rate: 10 cm^3/h, gas flow rate: 1 cm^3/min.

Orientation of the residence time loop

For the reason of also using relatively low flow rates of liquid and gas, the differences between a setup with horizontal and vertical orientation of the glass tube were investigated. On the one hand, a vertically stored tube is a less footprint consuming setup in laboratory but on the other hand the liquid flow has to be accelerated by the gas flow against gravity or has to overcompensate the buoyancy of the gas bubbles, depending on the flow direction in the case of a vertical tube. The results for these experiments are given in Figure 8 and Table 1.

Using a nitrogen flow of 1 cm^3/min and liquid flow of 10 cm^3/h in a vertically stored tube with an upward flow direction all characteristic parameters, including the mean residence time, show significant deviations from the experiment with a horizontal tube. In particular, the dimensionless variance for the vertical tube setup is fivefold higher than that for a horizontally stored tube. The latter exhibits a variance (as a measure of the spread of the response signal) eight times smaller than that of the vertical tube.

In the case of a vertical tube with a downward directed flow the response signal shows a distinctive greater tailing. Because of this, the maximum of the corresponding dimensionless exit age distribution function shifts to the left (Figure 8). This is accompanied by smaller mean residence times. Furthermore, both the variance and the dimensionless variance are significantly greater (Table 1).

If the gas flow is reduced to 0.5 cm^3/min the dimensionless exit age distribution function of the setup with a downward

Table 1. Comparison of Vertically Oriented Mixer-Tube Setups with a Horizontally Oriented Setup*

Orientation of the Glass Tube	$\bar{t}$/min	σ_t^2/min^2	σ_θ^2
Horizontal	5.30	0.044	0.0015
Vertical upward	6.84	0.373	0.0080
Vertical downward	4.90	0.673	0.0280

*Liquid flow 10 cm^3/h, gas flow 1 cm^3/min, tube 150 cm.

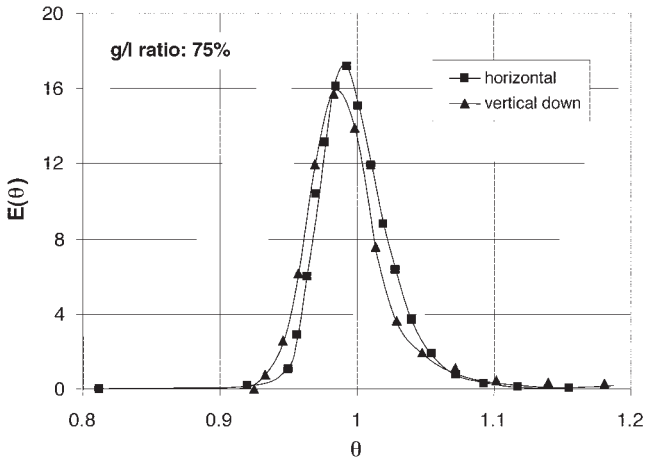

Figure 9. Dimensionless exit age distribution functions of setups with different stored glass tubes.

Length: 150 cm, liquid flow rate: 10 cm^3/h, gas flow rate: 0.5 cm^3/min.

flow shows a course similar to that of the horizontal setup (Figure 9). This improvement could be explained by the reduced buoyancy present, attributed to the lower gas flow. It should be noted that an experiment with the reverse flow direction at these flow rates was not feasible because of accumulation of the liquid phase in the tube.

Because the mean residence times of these experiments are different (Table 1), a validation of the setup was carried out. For this purpose, the mass flow of the setup was determined for different time intervals and various flow conditions. For analysis, the ratios of the weight of the collected samples to the known flow rate were compared with the time intervals of sample collection. The results are given in Figure 10.

The top graph in Figure 10 shows deviations between the expected times calculated from the collected weights and the measured times for a vertical tube setup and shows that this setup does not run in a steady state if a liquid flow rate of 10 cm^3/h in combination with a gas flow rate of 1 cm^3/min is used. Further experiments show that these deviations could be minimized if higher total flow rates (such as 1,000 cm^3/h for liquid flow and 50 cm^3/min for gas flow) are used. Another possibility to attain a steady state of the dispersion flow in the vertical tube setup is to increase the rigidity of the foam by increasing the gas flow rate (such as from 1 to 2 cm^3/min), leaving the liquid flow rate constant at 10 cm^3/h. Depending on hydrostatic pressure, deviations cannot be observed if a horizontal tube setup is used, as shown in the bottom graph of Figure 10. In addition the setup with the vertical tube and a downward directed flow shows no divergence between the experimentally determined and theoretically calculated mass flow.

Comparison between low and high total flow rates

Two experiments were performed, one at low and the other at high liquid flow rates. The low flow rate experiment (10 cm^3/h liquid flow, 0.5 cm^3/min gas flow) was already presented above in Figure 3. The liquid flow rate of 10 cm^3/h had also been applied in all other experiments previously described. The second experiment was performed at a much higher liquid flow rate of 1000 cm^3/h and a gas flow of 50 cm^3/min. The gas/liquid ratio is thus kept constant.

Comparison between the flows is based, first, on the changes in the system's pressure drop with consequences on the bubble size and arrangement and, second, on the effects of the liquid velocity within the capillary on the dispersion.

The major difference between the experiments with low (Figure 3) and high (Figure 11) total flow rates is, besides the absolute time scale, a conspicuously greater flattening of the exit age distribution function in the case of the higher flow rate. The dimensionless exit age distribution functions (Figure 12) allow a direct comparison of these experiments and clearly confirm this result. It can be seen that the overall dimensionless variance is approximately 20 times greater in the case of the higher total flow rate.

Because the total flow rate affects the pressure drop of the setup and thereby the gas volume of the bubbles, the relationship between the dimensionless variances in dependency of the

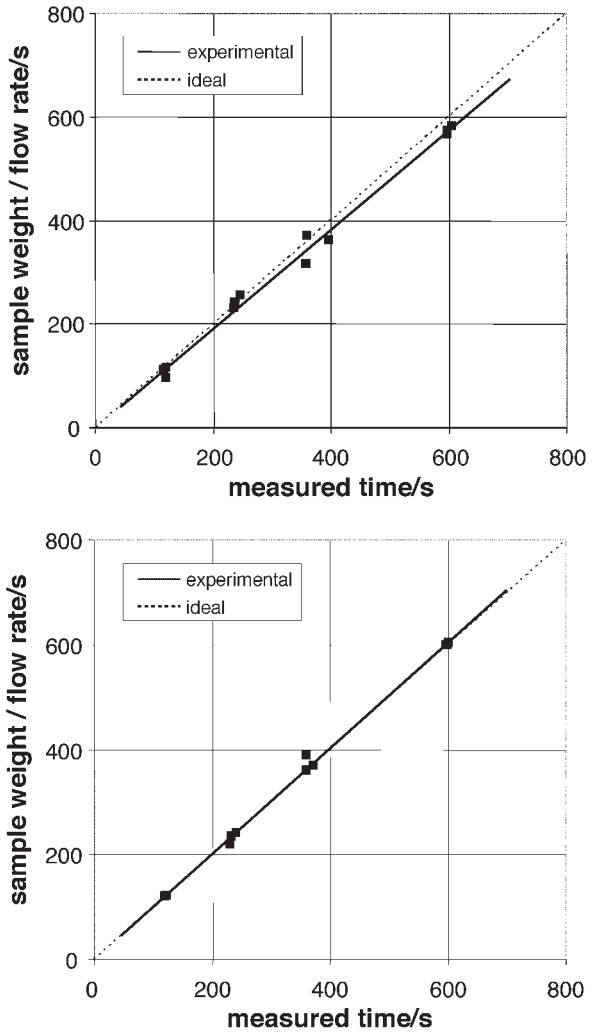

Figure 10. Setup validation by comparison of the ratios of sample weight to flow rate with the time intervals of sample collection.

Top: vertical tube, liquid flow 10 cm^3/h, gas flow 1 cm^3/min; bottom: horizontal tube, liquid flow 10 cm^3/h, gas flow 1 cm^3/min.

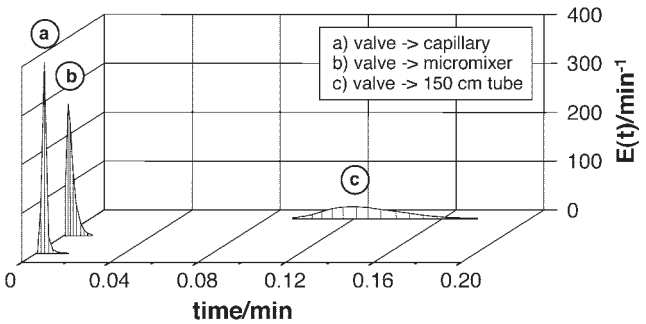

Figure 11. Exit age distribution function at different measuring points of the horizontal screening setup with 1,000 cm^3/h liquid flow rate and 50 cm^3/min gas flow rate.

total flow rate and the pressure drop is investigated. For this purpose the pressure drop of the setup is measured at the gas inlet of the mixer, which has either a connected or a disconnected tube.

From Table 2, it can be seen that for an increased flow rate, by a factor of 100, the individual contribution of the micromixer toward the overall pressure drop is increased. For a low total flow rate the ratio of the individual contribution of the micromixer and the tube is 1.6 (Table 2, No. 1). In the case of the higher flow rate (No. 5), this ratio is increased to 9.4.

A further relationship that can be achieved from Table 2 is the faster increasing pressure drop of the tube, compared to the micromixer, if the liquid flow is constant at 10 cm^3/h and the gas flow rate is increased from 0.5 up to 4 cm^3/min (Nos. 1–4). If a gas flow rate of 1 cm^3/min (No. 2) is used, the achieved pressure drops in the micromixer and the tube are nearly equal. For higher gas flow rates [such as 2 cm^3/min (No. 3)], the pressure drop in the tube exceeds that of the micromixer.

Figure 13 shows the impact of the change of the flow rate when adding the components, particularly referring to the "valve/capillary." Although the overall contribution of the "valve/capillary" is small (compared to that of the other components), it is clear that the dimensionless variance is much larger at low than at high flow rates.

This stems from the known different axial and radial dispersion of tubes depending on the velocity profile of a single-phase liquid flow. The two total flow rates differ by a factor 100. The liquid flow rate of 10 and 1,000 cm^3/h in the steel capillary correspond to Reynolds numbers of approximately 6 and 590, respectively. Although both flows are in the laminar regime it can be assumed that the differences in the dimensionless variances with regard to the "valve/capillary" result from dispersion effects in the capillary as a function of the flow rate.

Discussion

Although previous practical experience (de Bellefon et al., 2000) showed that foams made of micromixers are very efficient carriers for pulse investigations, the present study shows more subtle details on how to further optimize this pulse carriage, in particular on how to reduce pulse broadening by considering all contributions with the total screening system. Within this context, for an improvement of the screening setup in terms of increasing the number of experiments per time, it was shown that it is also important to use a valve optimized with respect to dead volumes and a capillary as short as possible to minimize the pulse broadening before the dispersion is generated. Furthermore, the volume of the tracer input should be minimized as much as possible.

Admittedly, the main efforts on optimization, especially for setups with short tubes, should be focused on the micromixer and the tube. The dimensionless variances of the micromixer depicted in the bottom graph of Figure 4 as well as the vessel number of one calculated by the application of the tanks-in-series model indicate that the micromixer has the greatest relative stake in signal dispersion with respect to the residence time. Therefore a device optimization should be focused on the micromixer. In contrast, the optimization efforts regarding the process parameters should be focused on the tube, given that the main absolute contribution toward signal broadening results from it (Figure 4, top).

Furthermore, the investigations of the exit age distribution functions and the calculation of the variances indicate that it is necessary to use relatively low total flow rates and a gas/liquid ratio not too dissimilar from the density ratio of a face-centered cubic or hexagonal lattice to minimize the principal amount of the dimensionless variance of the micromixer as well as the overall variance of the setup.

Contrary to expectations, a greater rigidity of the foam resulting from a higher gas/liquid ratio adversely affects the signal broadening. The experimental results illustrated in Figure 6 indicate that the broadening of the signal is increased with a higher gas/liquid ratio. This could possibly be the consequence of the limited particle transport by diffusion in a drained foam. For example, if the laminar liquid film at the surface of the glass tube or of the outlet slit of the mixer is dyed with methyl blue, it should take more time for the dye molecules to diffuse back into the liquid-filled interstitials of the foam stream at higher gas/liquid ratios because in this case both the volume of these liquid-filled interstitials and the contact frequency between these interstitials and the laminar film are clearly smaller.

Regarding the orientation of the glass tube, a significantly smaller variance as well as dimensionless variance of the glass

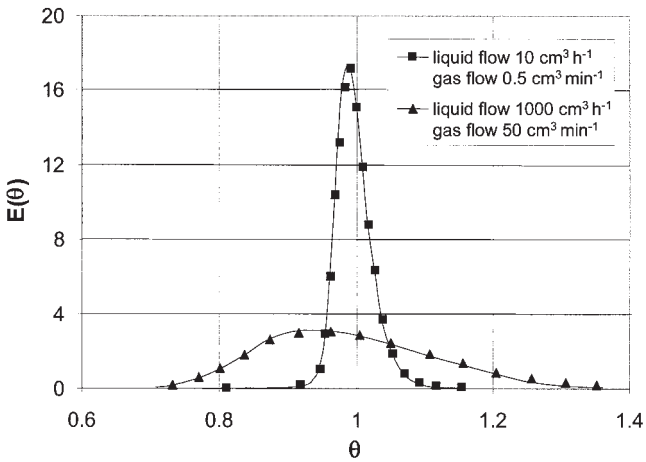

Figure 12. Dimensionless exit age distribution functions with high and low total flow rate.

Table 2. Pressure Drop of the Setup with a Connected and Disconnected Horizontal 150-cm Tube Using Different Total Flow Rates

No.	Liquid/cm^3/h^{-1}	Gas/cm^3/min^{-1}	Pressure Drop		
			Mixer and Tube/kPa	Mixer/kPa	Tube/kPa
1	10	0.5	5.0	3.1	1.9
2	10	1	8.1	4.4	3.7
3	10	2	14.2	6.4	7.8
4	10	4	27.8	10.9	16.9
5	1000	50	195.2	176.5	18.8

tube at low total flow rates was obtained in the case of a horizontal orientation. It is assumed that in the case of a horizontal orientation the effect of gravity on the liquid phase is minimized. Validation experiments comparing the ratio of sample weight to flow rate with the time intervals of the sample collection indicated that, in the case of low total flow rates, no accumulation of liquid in the setup with horizontally orientated tube occurs, whereas the opposite is true for vertical orientation with upward directed flow.

Validation of the setup with a vertical tube and a downward directed flow also indicates a stationary state similar to that using a horizontal tube. Nevertheless, the smaller mean residence time indicates acceleration of the liquid phase attributed to gravity. Especially at higher gas/liquid ratios this acceleration leads to higher variances, as depicted in Figure 8 and Table 1. It appears that in the case of a downward directed flow the upward striving bubbles act like miniature mixers.

The total flow rate and the subsequent pressure drop also exert an influence toward signal broadening. The increased pressure drop at higher flow rates induces a reduction of the total volume of the gas phase in the mixer-tube setup. In particular at higher total flow rates, this pressure gradient leads to a significant alteration of the gas/liquid ratio of the foam during its way through the setup. Because of the decreased total volume, the resulting smaller gas bubbles reduce the rigidity of the foam and lead to an increased signal broadening. Therefore, a low pressure drop of the setup should be favored to achieve further minimization of the signal broadening.

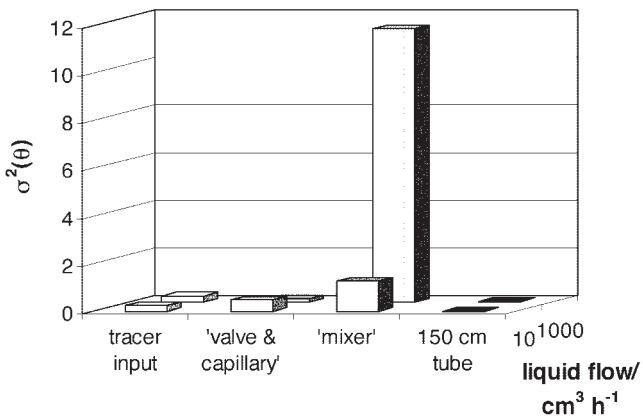

Figure 13. Dimensionless variances of the individual components at high and low total flow rate.

High: liquid flow: 1,000 cm^3/h, gas flow: 50 cm^3/min. Low: liquid flow: 10 cm^3/h, gas flow: 0.5 cm^3/min.

Outlook and Conclusions

Some of the conclusions drawn above can be used directly and without major technical expenditure to optimize serial transient screening setups based on mixer/tube setups, such as the one at CNRS in Lyon (de Bellefon et al., 2000). For instance, the horizontal orientation of the glass tube meanwhile was adapted in the screening setup at the Lyon site and will be used in future reaction processing for finding catalysts. More elaborate, but still within reach, is the development of novel micromixers specially developed for pulse operation, in that it was shown that these devices have the predominant contribution with respect to the dimensionless exit age distribution $E(\theta)$. In turn, the greatest contribution for the exit age distribution $E(t)$ was conferred by the tube. Here, a modification of the foam structure by changing its composition to match the surface, surface tension, and density is required. This is regarded as a rather complex optimization step.

Most important, the results have shown that the current lower limit for a sampling period of 12 min for gas/liquid phase screening can be overcome with substantial improvement and that, despite screening apparatus optimization, the improvement of process parameters, particularly for achieving more defined hydrodynamics, is a key for advanced serial catalyst screening using mixer/tube reactor setups.

Acknowledgments

The authors thank the European Commission for funding this work, which was carried out within the EU Project Key Elements for the Application of Microreactors in Multiphasic Catalytic Chemistries (KEMiCC), under Project Grant G1RD-CT2000-00469.

Literature Cited

Aris, R., "On the Dispersion of a Solute in a Fluid Flowing through a Tube," *Proc. R. Soc. Lond.*, 67 (1955).

Besser, R. S., J. Fort, H. Surangalikar, and S. Ouyang, "Microdevice-Based System for Rapid Catalyst Development," Proc. of 5th Int. Conf. on Microreaction Technology: IMRET 5, M. Matlosz, W. Ehrfeld, and J. P. Baselt, eds., Springer-Verlag, Berlin, pp. 499–507 (2001).

Besser, R., and M. Prevot, "Linear Scale-up of Micro Reaction Systems," Proc. of 4th Int. Conf. on Microreaction Technology: IMRET 4, Mar. 5–9, Atlanta, GA, pp. 278–283 (2000).

Cong, P., R. D. Doolen, Q. Fan, D. M. Giaquinta, S. Guan, E. W. McFarland, D. M. Poojary, K. Self, H. W. Turner, and W. H. Weinberg, "High-Throughput Synthesis and Screening of Combinatorial Heterogeneous Catalyst Libraries," *Angew. Chem. Int. Ed.* **38**(4), 484 (1999).

de Bellefon, C., N. Pestre, T. Lamouille, P. Grenouillet, and V. Hessel, "High Throughput Kinetic Investigations of Asymmetric Hydrogenations with Microdevices," *Adv. Synth. Catal.*, **345**(1/2), 190 (2003).

de Bellefon, C., N. Tanchoux, S. Caravieilhes, P. Grenouillet, and V. Hessel, "Microreactors for Dynamic High Throughput Screening of

Fluid/Liquid Molecular Catalysis," *Angew. Chem. Int. Ed. Engl.*, **39**(19), 3442 (2000).
Ehrfeld, W., K. Golbig, V. Hessel, H. Löwe, and T. Richter, "Characterization of Mixing in Micromixers by a Test Reaction: Single Mixing Units and Mixer Arrays," *Ind. Eng. Chem. Res.*, **38**(3), 1075 (1999).
Haverkamp, V., W. Ehrfeld, K. Gebauer, V. Hessel, H. Löwe, T. Richter, and C. Wille, "The Potential of Micromixers for Contacting of Disperse Liquid Phases," *Fresenius' J. Anal. Chem.*, **364**, 617 (1999).
Herweck, T., S. Hardt, V. Hessel, H. Löwe, C. Hofmann, F. Weise, T. Dietrich, and A. Freitag, "Visualization of Flow Patterns and Chemical Synthesis in Transparent Micromixers," Proc. of 5th Int. Conf. on Microreaction Technology: IMRET 5, M. Matlosz, W. Ehrfeld, and J. P. Baselt, eds., Springer-Verlag, Berlin, pp. 215–229 (2001).
Hessel, V., W. Ehrfeld, K. Golbig, V. Haverkamp, H. Löwe, and T. Richter, "Gas/Liquid Dispersion Process in Micromixers: The Hexagon Flow," Proc. of 2nd Int. Conf. on Microreaction Technology: IMRET 2, February, New Orleans, LA (1998).
Hessel, V., W. Ehrfeld, V. Haverkamp, H. Löwe, and J. Schiewe, *Dispersion Techniques for Laboratory and Industrial Production*, R. H. Müller, ed., Apothekerverlag, Stuttgart, Germany (1999).
Hoffmann, C., H.-W. Schmidt, and F. Schüth, "A Multipurpose Parallelized 49-Channel Reactor for the Screening of Catalysts: Methane Oxidation as the Example Reaction," *J. Catal.*, **198**, 348 (2001).
Hoffmann, C., A. Wolf, and F. Schüth, "Parallel Synthesis and Testing of Catalysts under Nearly Conventional Testing Conditions," *Angew. Chem. Int. Ed. Engl.*, **38**(18), 2800 (1999).
Liauw, M., M. Baerns, R. Broucek, O. V. Buyevskaya, J.-M. Commenge, J.-P. Corriou, L. Falk, K. Gebauer, H. J. Hefter, O.-U. Langer, H. Löwe, M. Matlosz, A. Renken, A. Rouge, R. Schenk, N. Steinfeld, and S. Walter, "Periodic Operation in Microchannel Reactors," Proc. of 3rd Int. Conf. on Microreaction Technology: IMRET 3, W. Ehrfeld, ed., Springer-Verlag, Berlin, pp. 224–234 (2000).
Mathes, H., and P. J. Plath, "Generation of Monodisperse Foams Using a Microstructured Static Mixer," Tunisian–German Conference: Smart Systems and Devices, Mar. 27–30, Hammamet, Tunisia (2001).
Rodemerck, U., P. Ignaszewski, M. Lucas, P. Claus, and M. Baerns, "Parallel Synthesis and Testing of Heterogeneous Catalysts," Proc. of 3rd Int. Conf. on Microreaction Technology: IMRET 3, W. Ehrfeld, ed., Springer-Verlag, Berlin, pp. 287–293 (2000).
Taylor, Sir G., "The Dispersion of Matter in Turbulent Flow through a Pipe," *Proc. R. Soc. London Ser. A*, **223**, 446 (1954).
Thomson, S., C. S. R. Hoffmann, H.-W. Schmidt, and F. Schüth, "The Development of a High-Throughput Reactor for the Catalytic Screening of Three Gas Phase Reactions," *Appl. Catal. A: Gen.*, **220**(1/2), 253 (2001).
Walter, S., E. Joannet, M. Schiel, I. Boullet, R. Philipps, and M. Liauw, "Microchannel Reactor for the Partial Oxidation of Isoprene," Proc. of 5th Int. Conf. on Microreaction Technology: IMRET 5, M. Matlosz, W. Ehrfeld, and J. P. Baselt, eds., Springer-Verlag, Berlin, pp. 387–396 (2001).
Walter, S., and M. Liauw, "Fast Concentration Cycling in Microchannel Reactors," Proc. of 4th Int. Conf. on Microreaction Technology: IMRET 4, Mar. 5–9, Atlanta, GA, pp. 209–214 (2000).
Zech, T., D. Hönicke, J. Klein, S. Schunk, and D. Demuth, "A Novel System Architecture for High-Throughput Primary Screening of Heterogeneous Catalysts," Proc. of 5th Int. Conf. on Microreaction Technology: IMRET 5, May 27–30, Strasbourg, France (2001).
Zech, T., D. Hönicke, A. Lohf, K. Golbig, and T. Richter, "Simultaneous Screening of Catalysts in Microchannels: Methodology and Experimental Setup," Proc. of 3rd Int. Conf. on Microreaction Technology: IMRET 3, Frankfurt, Germany (1999).

Manuscript received Jan. 24, 2003, and revision received Oct. 27, 2003.